COMPUTER-AIDED DIAGNOSIS APPLIED TO MRI IMAGES OF BRAIN TUMOR USING SPATIAL FUZZY LEVEL SET AND ANN CLASSIFIER

VIRUPAKSHAPPA S[*], SACHINKUMAR VEERASHETTY[†], AND AMBIKA N[‡]

Abstract. The most vital organs in the human body are the brain, heart, and lungs. Because the brain controls and coordinates the operations of all other organs, normal brain function is vital. Brain tumour is a mass of tissues which interrupts the normal functioning of the brain, if left untreated will lead to the death of the subject. The classification of multiclass brain tumours using spatial fuzzy based level sets and artificial neural network (ANN) techniques is proposed in this paper. In the proposed method, images are preprocessed using Median Filtering technique, the boundaries of the Brain Tumor are obtained using Spatial Fuzzy based Level Set method, features are extracted using Gabor Wavelet and Gray-Level Run Length Matrix (GLRLM) methods. Finally ANN technique is used for the classification of the image into Normal or Benign Tumor or Malignant Tumor. The proposed method was implemented in the MATLAB working platform and achieved classification accuracy of 94%, which is significant compared to state-of-the-art classification techniques. Thus, the proposed method assist in differentiating between benign and malignant brain tumours, enabling doctors to provide adequate treatment.

Key words: Median Filter, Spatial Fuzzy Level Set, GLRLM, Gabor features, Artificial Neural Networks, Benign, Malignant and Computer-aided Diagnosis (CAD) system.

AMS subject classifications. 68T05

1. Introduction. Various Medical Imaging technique are used to produce the images of human body. The medical experts provide the treatment by observing and analysing those images [1]. Different medical imaging techniques being used in daily life are Magnetic Resonance Imaging (MRI), Computerized Tomography, Ultrasonic and X-ray [2, 3] which applied individually through variety of sensory systems. Medical imaging also helps doctor in viewing inner portions of the body and diagnose properly. Doctors also gets help in making keyhole surgery where interior parts can be operated easily without opening the body more.

The neuroscience field has seen a significant increase in demand for medical image analysis over the past 20 years. Higher resolution and contrast ratio images of the internal organs and tissues are produced by MRI imaging. The anatomical structural details are also provided by the nuclear magnetic resonance theory. The contrast ratio between various interstitial fluids will vary depending on the variety of imaging sequences. The signals from magnetic particles spinning in the body in accordance with its magnetic tune are picked up by a powerful computer during an MRI scan, which transforms the scanned data into visual representations of the internal body parts. Medical imaging results can be modified to take advantage of the imaging techniques used in the development of the analysis of remote sensing data and to easily analyse the symptoms of patients [4].

All neutrons, electrons, and protons move in a circular motion because they all have an angular moment around their respective axes. The magnetic field that surrounds all charged objects is created by their odd mass number and circular spin. When an external force is acting on these tiny magnetic fields that are randomly aligned, the MRI machine uses these magnetic fields to generate signals. Tiny magnetic fields automatically align with stronger ones if they are contained by larger homogeneous magnetic fields. This is how MRI works. In fact, the majority of the atoms in the human body are hydrogen, and each one of these atoms contains a single proton in the nucleus. MRI machines are therefore more sensitive to hydrogen.

Together with advances in medical imaging technology, neuroscientists are becoming more interested in techniques or methodologies for identifying normal tissues in the brain in order to improve the effectiveness

---

[*]Department of CSE, Sharnbasva University, Kalaburagi, Karnataka, India (`virupakshi.108@gmail.com`).

[†]Department of CSE, Sharnbasva University, Kalaburagi, Karnataka, India.(`sveerashetty@gmail.com`).

[‡]Department of CSE, Sharnbasva University, Kalaburagi, Karnataka, India (`ambika.umashetty@gmail.com`).

of therapy for brain disease [5]. It is difficult to diagnose and perform surgery on the brain, which is located inside the cranium. A non-obtrusive approach to diagnosis has become the standard practice, and its use has swept the globe. A brain tumour is one of the most dangerous diseases. The primary issue in brain tumour treatment is its location and its capacity to spread rapidly. Thus, the critical steps in addressing this issue are segmenting the image and identifying them [6, 7].

Medical image segmentation is one of the most important branches of image segmentation, and it is the first and most important step in medical image analysis. The advancement of magnetic resonance imaging in 3D space allows for the imaging of tissues with high contrast and resolution. The neuroscientist observes three important parts of the brain: cerebrospinal fluid, white matter, and grey matter. Morphological structures are the fundamentals of these studies, which are used to segment medical images. For testing purposes, the technique of medical image segmentation provides automatic and semiautomatic tumour extraction methods.

2. Literature survey. Yash Sharma et al [8] proposed a novel boundary box method for brain tumor detection named as Fast Bounding Box (FBB). This method helps in locating the tumors in the brain from MRI image of patient's brain. This is used to find out most dissimilar brain region called as the Region of Interest (ROI) i.e. tumor location. The FBB make use of novel score function known as Bhattacharya's Coefficient (BC) for axes points of the bounding box in which tumor region is inscribed and is different from other regions of the image. The FBB finds out the most dissimilar portion properly but sometimes fails to find out some tumour's tissue which is easily available and it might be the part of tumor region. In order to reduce this, the region of ROI is scaled up to 20 pixels which lead to enhanced ROI. This increases the size of the bounding box by 20 pixels on each side increasing the area so that if tumor part is left, it can also be covered in this process. The steps of this work are locating the tumor region using FBB and enhancing of ROI by scaling the bounding box. The ten features considered for the ANN training and GLCM feature provides 8 features.

Tianming Zhan et al [9] made use of fully automatic method in order to obtain the segmentation of tumor from multispectral MR images of the brain. They used different intensity patches in the input image for representing the abnormal and normal tissues. Dictionary is generated for further classification of tissues. The brain tumor and the normal brain tissue is classified by using the sparse representation classification in the complete image. Finally, regularisation of Markov Random Field (MRF) is used.

Kalyani A et al [10] presents neural network based classification of MRI brain images. The work consisted of three stages which are feature extraction, stage of feature reduction and finally classification. Initially, options with respective to tomography victimized images are obtained by Discrete Wavelet Transformation (DWT). The second stage deals with reduction of victimized principles part analysis to more essential options using PCA technique. In the classification stage, the two supervised machine learning based classifiers are used, the first one is feed forward neural network and second one is the back propagation neural network.

Apurva et al [11] has concentrated on detecting and classifying the tumor types like meningiomas, gliomas, nerve sheath and pituitary adenomas from MRI images of brain. The images in training phase and testing phase are pre-processed and segmented using adaptive K-means clustering. The segmentation process is followed by feature extraction using GLCM and Gabor wavelet methods. The classifier accuracy is improved by selecting the features using PCA algorithm. Multilevel Proximal Support Vector Machine (PSVM) classifier for detecting the different tumor types automatically from MRI images of brain.

V Sheejakumari et al [12] introduced Histon based technique for segmentation of the image. Before segmentation, noise is eliminated at the preprocessing stage by applying median filter. Then noise eliminated image is passed to the process of feature extraction. The features extracted are correlation, area, covariance and mean of images. The image classification is associated with neural network at final stage. Here neural network is modified by optimizing the values of weight using optimization technique called Artificial Bee Colony (ABC).

Jokin et al [13] proposed a hybrid method for classification of brain tumor in the MRI images. They removed the Noise using the median filter, extracted the texture features, used CART and SVM for hybrid classification.

P. Kumar et al [14] includes four stages in the work. They are preprocessing of the image, segmentation, extraction of the feature, feature reduction and finally classification. The Wiener filter is applied in preprocessing to reduce noise and further to extract features. Segmentation based on modified region growing is applied. Co-occurrence matrix and Histogram methods are utilized to extract edge and texture features. The feature space
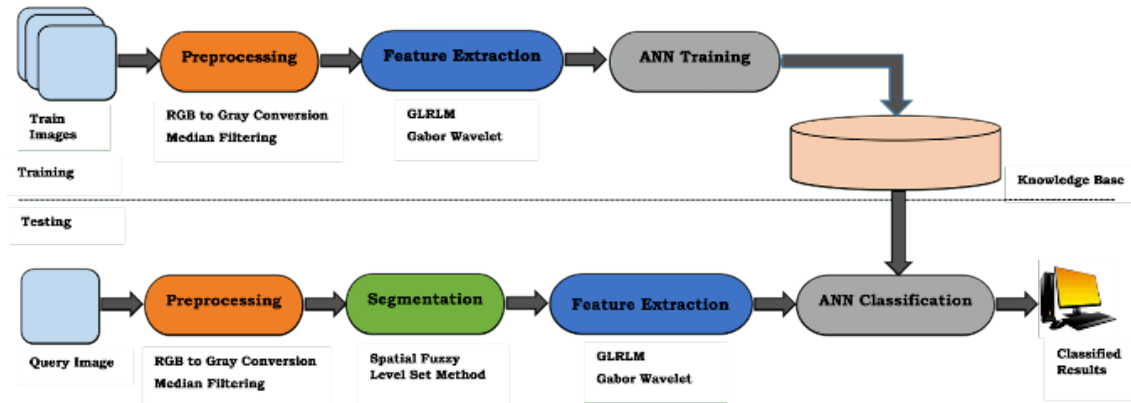
Fig. 3.1: Block Diagram of Proposed System

dimension is reduced by PCA to get efficient and better classification results. Kernel based SVM is used to classify them into Benign and Malignant. The similarity index, extra fraction and overlap fraction are measured for performance analysis.

Nithyapriya et al [15] used multifractional Brownian motion (mBm) to analyse the MRI brain images. Using mBm helps to extract spatially varying features. Depending upon multifractal features, segmentation process is carried. This is carried out using modified AdaBoost algorithm which is referred as Adaboost Support Vector Machine (SVM).

Marco Alfonse et al [16] used brain images of DICOM standard format to classify them into benign and malignant. Different phases considered are acquisition of data, preprocessing of data, Expectation Maximization and adaptive thresholding based segmentation, FFT based Features for MRI images, Minimal-Redundancy-Maximal-Relevance (MRMR) criteria based feature selection for valuable feature selection and the SVM for classification stage is used.

Deepa et al [17] used MEM approach for segmentation. The brain has different regions controlling different functions like speech, balance and movement. If any region gets damage it affects functionality of respective functions and may lose coordination of all activities. Brain tumor is nothing but tissue's abnormal growth in brain. If proper treatment to that tissue is failed, it spreads it to other tissue and results in cancer. Modified Expectation Maximization (MEM) is implemented in proposed method for segmentation and image is classified by SVM classifier. Correlation and Energy are calculated for the proposed work and are compared with existing methods.

3. Methodology. The Proposed work uses the Spatial Fuzzy Level Set Algorithm for Tumor Segmentation and GLRLM and Gabor wavelet features are used for feature extraction and ANN classifies into benign and malignant.

In pre-processing step, in order to reduce the computation complexity, input image is converted into monochrome image by using RGB to Gray conversion method and median filter is applied to eliminate noise present in the MRI image.

3.1. Median Filter. This filter is one of the non-linear filters used to eliminate the noise from the image while preserving the edges. This filter is applied by moving pixel by pixel in the image, its value is substituted by the value of median to its neighbors. The pattern of the neighbor considered is referred to as window which slides over the entire image on pixel by pixel basis. Values of window pixels are first arranged into numerical then median is calculated, this replaces the value of pixel being considered.

The median filter is similarly to mean filterwhich decreases the noise of the image. The median filter preserves the useful information in the image. This filter also comes under edge preserving smoothing filters.
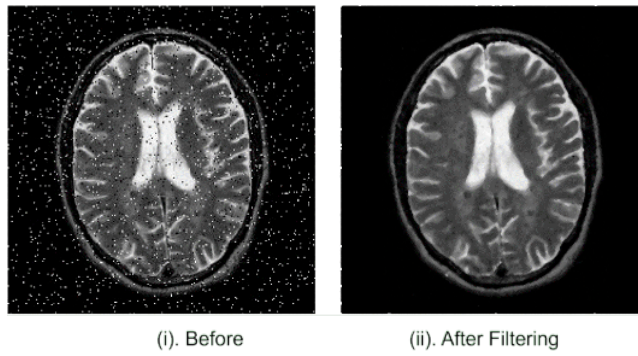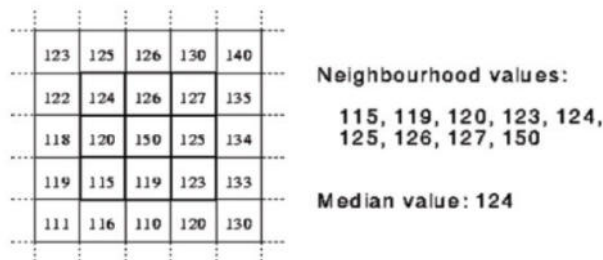
Fig. 3.2: Example for Median Filtering

Fig. 3.3: Median value estimation for each pixel neighbourhood.

For image $A(x)$ and the image $B(x)$, the constraint of median is as in the Equation (3.1).

$$median \ [\ A\ (x)\ +\ B\ (x)] \ \neq\ median\ [\ A\,(x)] \ +\ median\ [\ B\ (x)] \tag{3.1}$$

The filter smoothens the data retaining the small and sharper information. The median value is nothing but middle value of the neighbor pixel values. It is necessary to notice that this is equal to average or the mean value, rather the median value has half of the neighbourhood values greater than its value and rest half lesser than median value. It is stronger middle representative than that of average. Thus it is effective in eliminating various noises from the image [18].

In the above window, the central pixel has different value from the neighbouring pixels; therefore, median value is substituted. The above window's median value is 124. The Window of size 3×3 is used in this case.

3.2. Spatial Fuzzy Level Set Algorithm. Fixed cost function is reduced by adaptive estimation of scope of subclass and centroid in the fuzzy clustering, so it is adaptive kind of thresholding. Among fuzzy clustering, Fuzzy c-means (FCM) is popularly used algorithm and is widely used in the medical field.

A membership function $\mu_{m,n}$ is used in FCM to represent membership degree from mth cluster to nth object. it is mainly used in medical image segmentation as physiological tissues are non-homogeneous. FCM's cost function is given by Equation (3.2):

$$j\ =\ \sum_{m=1}^{K} \sum_{n=1}^{N} \mu_{mn}^{l} \|i_n - v_m\|^2 \tag{3.2}$$

The fuzziness of segmentation is controlled by the parameter $l > 1$. The following are constraints must have

subjected by the membership functions as given in Equation (3.3):

$$\sum_{m=1}^{c} \mu_{mn} = 1; \quad 0 \leq \mu_{mn} \leq 1; \qquad \sum_{n=1}^{N} \mu_{mn} > 0 \tag{3.3}$$

The centroids v_m and μ_{mn} must be iteratively updated as shown in the Equation (3.4) and (3.5):

$$\mu_{mn} = \frac{\|i_n - v_m\|^{-2/(l-1)}}{\sum_{k=1}^{c} \|i_n - v_k\|^{-2/(l-1)}} \tag{3.4}$$

$$v_i = \frac{\sum_{n=1}^{N} \mu_{mn}^{l} i_n}{\sum_{n=1}^{N} \mu_{mn}^{l}} \tag{3.5}$$

Later spatial FCM was proposed by Chuang and others in which the fuzzy membership functions can be incorporated by the spatial information directly by the following Equation (3.6):

$$\mu'_{mn} = \frac{\mu_{mn}^{P} h_{mn}^{q}}{\sum_{k=1}^{C} \mu_{kn}^{P} h_{kn}^{q}} \tag{3.6}$$

The parameters which control the respective contribution are p and q. The h_{mn} will add the spatial information as follows in given by the Equation (3.7):

$$h_{mn} = \sum_{k \in N_n} \mu_{nk} \tag{3.7}$$

N_n represents the local window with image pixel n as circle. The centroid v_m and weight μ_{mn} are updated according to the Equations (3.4) and (3.5). In pixel classification based on FCM, image is segmented using Level set method which employs dynamic variational boundaries. Active contour method is also very popular technique for image segmentation. But here, level set method embeds active contours to time dependent function of PDE $f(t, x, y)$ rather than the parametric characterization [19]. Then the active contour evolution can be approximated by orbiting at zero level set C(t) as in the Equation (3.8):

$$C(t) = \begin{cases} \phi(t, x, y) < 0 & (x, y) \text{ is inside } \Gamma(t) \\ \phi(t, x, y) = 0 & (x, y) \quad \text{ is at } \Gamma(t) \\ \phi(t, x, y) > 0 & (x, y) \text{ is outside } \Gamma(t) \end{cases} \tag{3.8}$$

Series of zero contours are comprised in the implicit interface C. Therefore the image segmentation is converted into $\cup S_k \cup \Gamma = 1$.

The Equation (3.9) determines the ϕ evolution using the equation of level set.

$$\begin{cases} \frac{\partial \phi}{\partial t} + F |\nabla \phi| = 0 \\ \phi(0, x, y) = \phi_0(x, y) \end{cases} \tag{3.9}$$

The normal direction is denoted by $|\nabla \phi|$, initial contour is represented by $\phi_0(x, y)$ and comprehensive forces is represented by F which also includes gradient image's external force, geometrical interface's internal force and optional artificial momentum.

The F advancing force need regularization using edge representative function g in the Equation (3.10) to pause the level set evolution till optimal solution is obtained.

$$g = \frac{1}{1 + |\nabla(G_\sigma * I)|^2} \tag{3.10}$$

where $G_\sigma * I$ represents the image convolution using Gaussian smoothing kernel G_s and image gadient is represented by ∇. The function g is approximal to zero in variational boundaries, else it will be positive.

In this medical image segmentation novel fuzzy based level set method is presented where it starts with clustering technique method called spatial fuzzy, then the results are further used to start the segmentation of the image, estimation of controlling parameters are carried out and evolution of the level set is regularized. The parameter initialization and configuration is automated by this new algorithm using spatial fuzzy. The spatial restrictions are employed with FCM for interested approximated contours determination in medical images [20]. The enhanced function of level set segmentation uses FCM output for evolution directly. Considering the interested component from FCM as $R_k : \{ r_k = \mu_{nk}, \ n = x \times N_y + y \}$. Now the level set will start conveniently as Equation (3.11):

$$\phi_0 (x, y) = - 4 \varepsilon (0.5 - B_k) \tag{3.11}$$

Here ε denotes a constant to regulate Dirac function. The Equation (3.12) defines this function as

$$\delta_\varepsilon (x) = \left\{ \begin{array}{ll} 0, & |x| > \varepsilon \\ \frac{1}{2\varepsilon} \left[1 + \cos \left(\frac{\pi x}{\varepsilon} \right) \right], & |x| \le \varepsilon \end{array} \right. \tag{3.12}$$

Binary image B_k is obtained from the Equation (3.13):

$$B_k = R_k \ge b_0 \tag{3.13}$$

where $b_0 (A(0,1))$ represent adjustable threshold. Given the initial level set function ϕ_0, the length and the area can be estimated using spatial fuzzy clustering

$$l = \int \delta (\phi_0) \, dxdy;$$

$$\alpha = \int H(\phi_0) dxdy$$

$H(\phi_0)$ is Heaviside function is defined according to Equation (3.14):

$$H (\phi_0) = \left\{ \begin{array}{ll} 1, & \phi_0 \ge 0 \\ 0, & \phi_0 < 0 \end{array} \right. \tag{3.14}$$

This segmentation algorithm considers the membership degree for every pixel of the image μ_k as the length for particular interested component R_k. The dynamic interface is pushed or pulled adaptively by the enhanced balloon force towards the interested object

$$G (R_k) = 1 - 2R_k \tag{3.15}$$

The result of balloon force $G (R_k) (\in [-1, 1])$ denotes a matrix having variable for pushing and pulling force to every pixel of the image. The interested object is attracted by the level set function irrespective to the initial position. As shown in the Equation (3.16), the evolution equation can be transformed into

$$\xi (g, \phi) = \lambda \delta (\phi) \ \mathrm{div} \left(g \frac{\nabla \phi}{|\nabla \phi|} \right) + g \ G (R_k) \ \delta (\phi) \tag{3.16}$$

3.3. Feature Extraction. The features used in this work are grey level run length matrix and Gabor Features.

3.3.1. Gray-level Run-length Matrix (GLRLM). The features for the texture analysis of the brain can be collected using GLRLM. The texture is analyzed by the pattern of grey value at certain angle in the direction of the reference pixels. The count of adjacent pixels having the similar grey value at certain direction is referred as Run length [21].
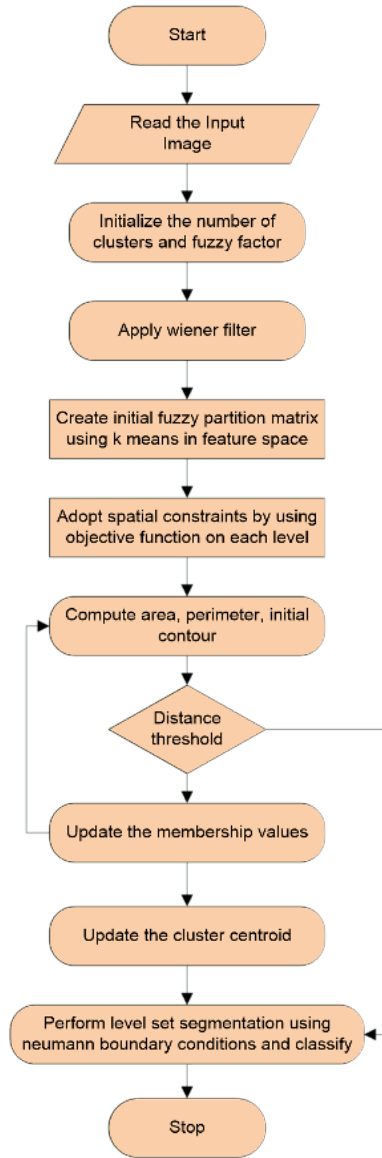
Fig. 3.4: Flow Chart of Fuzzy C Means With Spatial Constraints

GLRLM is a two dimensional matrix where each value is represented as p(i, j|θ) which gives the count of the elements j having the gray intensity i, in direction θ. Considering an example, figure 3.6 gives a 4×4 matrix of the pixel image having 4 different gray levels. The matrix given in figure 3.7 represents GLRLM with the direction of angle 0° [p(i, j|θ= 0°)].

The GLRL matrix can be constructed in the following orientations 0º, 45º, 90º as well as 135º. This is depicted below.

The texture features extracted from GLRLM [22] are

1. Shot Runs Emphasis(SRE):

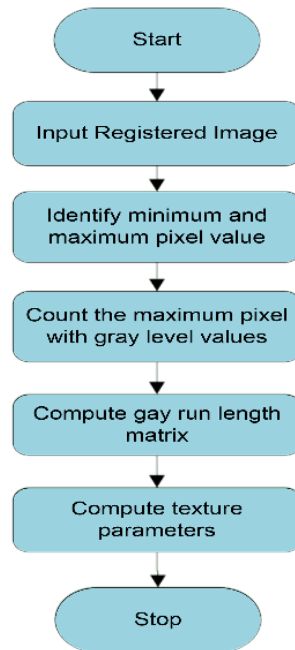$$SRE \; = \; \frac{1}{n} \sum_{i,j} \frac{p\;(\;i,j\;)}{j^2} \qquad (3.17)$$

Fig. 3.5: Flowchart for GLRLM Feature Extraction

Fig. 3.6: Matrix of Image 4×4 pixels

Fig. 3.7: GLRL Matrix

2. Long Runs Emphasis(LRE):

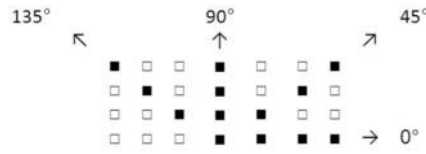$$LRE = \frac{1}{n} \sum_{i,j} j^2 \ p \ (\ i,j)$$
(3.18)

Fig. 3.8: Run Direction

3. Gray Level Non-uniformity(GLN):

$$GLN = \frac{1}{n} \sum_i \left(\sum_j p\ (x,y\ ) \right) 2 \tag{3.19}$$

4. Run Length Non-uniformity(RLN):

$$RLN = \ \frac{1}{n_r} \sum_{j=1}^{N} p_r\ (i)^2 \tag{3.20}$$

5. Run Percentage(RP):

$$RP\ = \sum_{i,j} \frac{n}{p\ (i,j)\,j} \tag{3.21}$$

6. Low Grey Level Run Emphasis(LGRE)

$$LGRE = \ \frac{1}{n} \sum_{i,j} \frac{p\ (i,j)}{i^2} \tag{3.22}$$

7. High Gray Level Run Emphasis(HGRE)

$$HGRE = \ \frac{1}{n} \sum_{i,j} i^2\ p\ (i,j) \tag{3.23}$$

3.3.2. Gabor Feature. The 2-D Gabor filter is represented by following Equation (3.24) and Equation (3.25):

$$h\left(x,y;f,\theta\right) = \ \frac{1}{\sqrt{\pi \sigma_1 \sigma_2}} \exp\left(-\frac{1}{2} \left(\frac{R_1^2}{\sigma_1^2} + \frac{R_2^2}{\sigma_2^2} \right) \right) .\exp\left(i\left(f_x x + f_y y \right) \right) \tag{3.24}$$

$$H\left(u,v;f,\theta\right) = \ 2\sqrt{\pi \sigma_1 \sigma_2} \exp\left(-\frac{1}{2} \left(\sigma_1^2 (S_1 - f)^2 + \sigma_2^2 S_2^2 \right) \right) \tag{3.25}$$

here $R_1 = $ x cos θ +ysin θ , $R_2 = -$x sin θ +ycos θ , $\sigma_1 = \frac{c_1}{f}$, $\sigma_2 = \frac{c_2}{f}$, $f_x = $ fcos θ , $f_y = $ fsin θ ,
$S_1 = $ u cos θ + v sin θ , $S_2 = -$u sin θ + v cos θ , c_1 and c_2 are constants.

The coefficient $\sqrt{\pi \sigma_1 \sigma_2}$ guarantees that different Gabor filter in the family have their energy equal to 1 i.e., $\|h\|^2 = \int \int$ hh*dxdy= 1.

The spatial sinusoids which are localized using Gaussian window are referred by Gabor filters and band pass filters, which are frequency sensitive and orientation. The x and y terms used in Eq. (3.24) are digital image pixel co-ordinates. The 2-D Gaussian standard envelope are represented by σ_1 and $\sigma_2$parameters. The f indicates the pass band central frequency and µ is the spatial orientation [23].

Considering $\sigma_1 = \sigma_2 = \sigma$, Equation (3.24) and Equation (3.25) can be simplified as Equation (3.26) and Equation (3.27):

$$h\ (x, y; f, \theta) = \ \frac{1}{\sqrt{\pi}\sigma}\exp\ \left(-\frac{x^2 + y^2}{2\sigma^2}\right)\ .\exp\ (i\ (f_x x + f_y y)) \tag{3.26}$$

$$H\ (u, v; f, \theta) = \ 2\sqrt{\pi}\sigma\exp\left(-\frac{\sigma^2\left((u - f_x)^2 + (v - f_y)^2\right)}{2}\right) \tag{3.27}$$

The Gabor filter is complex type with two components: real and imaginary

— The real part is $\frac{1}{\sqrt{\pi}\sigma_1\sigma_2}\exp\left(-\frac{1}{2}\left(\frac{R_1^2}{\sigma_1^2} + \frac{R_2^2}{\sigma_2^2}\right)\right)\cos(fR_1)$

— The imaginary is $\frac{1}{\sqrt{\pi}\sigma_1\sigma_2}\exp\left(-\frac{1}{2}\left(\frac{R_1^2}{\sigma_1^2} + \frac{R_2^2}{\sigma_2^2}\right)\right)\sin(fR_2)$

The family of Gabor filters takes both phase and amplitude of the frequency spectrum [24]. Gabor features are extracted by convolution of image I with all the Gabor filters family at each and every pixel (x, y) and is given by the Equation (3.28):

$$G\ (x, y, f_k, \theta_m) = \ \sum_{x'}\sum_{y'} I\ \left(x - x', y - y'\right)\ h\ (x', y'; f_k, \theta_m) \tag{3.28}$$

where $I(x, y)$ represents the intensity of the pixel.

The Gabor features used [24] are:

1. The phase feature of $G\ (f_k, \theta_m)$ can be represented by edge location and some other information of the image I as depicted by the Equation (3.29).

$$F_1\ (x, y; f_k, \theta_m) = \ \text{phase}\ (G\ (x, y; f_k, \theta_m)) \tag{3.29}$$

2. The amplitude feature of $G\ (f_k, \theta_m)$ is represented as oriented frequency spectrum of image I in every location as in Equation (3.30)

$$F_2\ (x, y; f_k, \theta_m) = |G\ (x, y; f_k, \theta_m)| \tag{3.30}$$

3. The sum of squares of various frequency responses having same orientation can be considered as feature and it also indicates the local energy of particular orientation given by Equation (3.31)

$$F_3\ (x, y; \theta_m) = F_2\ (x, y; f_0, \theta_m)^2 + \frac{1}{4}F_2\left(\left\lfloor\frac{x}{2}\right\rfloor, \left\lfloor\frac{y}{2}\right\rfloor; f_1, \theta_m\right)^2 + \frac{1}{16}F_2\left(\left\lfloor\frac{x}{4}\right\rfloor, \left\lfloor\frac{y}{4}\right\rfloor; f_2, \theta_m\right)^2 \tag{3.31}$$

In Eq. (3.31) $F_2\ (f_0, \theta_m)$ is a $\frac{X}{2} \times \frac{Y}{2}$ image, and $F_2\ (f_1, \theta_m)$ is a $\frac{x}{4} \times \frac{y}{4}$ image, and $F_2\ (f_2, \theta_m)$ is a $\frac{x}{8} \times \frac{y}{8}$ image. The $F_3\ (\theta_m)$ is a $\frac{X}{2} \times \frac{Y}{2}$ image, thus each pixel of $F_2\ (f_1, \theta_m)$ is further partitioned to 4 pixels and each pixels of $F_2\ (f_2, \theta_m)$ is partitioned equally into 16 pixels.

4. The orientation can also be considered as feature which is maximum local energy.

$$F_4\ (x, y) = k \tag{3.32}$$

Where $F_3\ (x, y; \theta_k) = \max_{m=0\sim2}\{F_3\ (x, y; \theta_m)\}$

Algorithm's Steps:

step-1: Select the value of F.

step-2: Convert the image to 2D matrix

step-3: Using the formula given below the impulse response is calculated

$$G\ (x, y) = g\ (x, y) \times \exp\{2\pi i f\ (x\cos\theta + y\sin\theta)\}$$

g is given as follows

$$g\ (x, y) = \left(\frac{1}{2\pi S^2}\right) \times \exp\{-\ (x^2 + y^2)\ /\ 2S^2\}$$
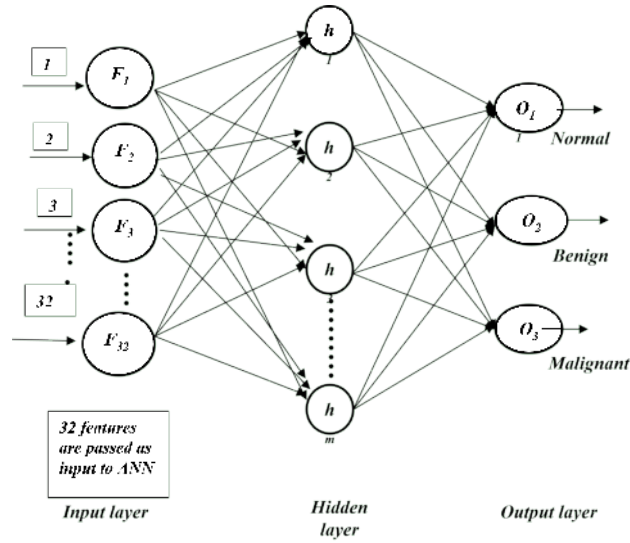
Fig. 3.9: Neural Network Structure

step-4: the image is passed to the filter having the impulse response as given in the step 3, filtered image is represented by $r(x, y)$.

step-5: The filtered image's energy is computed as $E = r2(x; y)$

step-6: From filtered image estimate the segmented image using.
$\varphi(x, y) = E \bigotimes m(x, y)$ mask window is denoted by $m(x, y)$. Using standard deviation Ss window size is estimated. we adopt Ss = S / Sigma. So,

$$m \ (\ x, y\ ) \ = \ \left(\frac{1}{8\pi\sigma^2} \right) * \exp\left\{ -\left(\frac{n12 \ + \ n22}{4\sigma^2} \right) \right\}$$

step-7: Print $\phi(x, y)$, i.e. output image.

3.4. Artificial Neural Networks (ANN). A neural network (ANN) is made up of a large number of highly interconnected processing elements known as neurons. The ANN's operations are divided into two phases: training and testing. The ANN is trained with specific input patterns during the training phase. When an instructed input pattern is detected at the input during the testing phase, an output is generated.

Figure 3.9 shows architecture of proposed three output Feed Forward Back Propagation Neural Network (FF-BPNN). The nodes F_1, F_2...F_{32} represent the corresponding input features and the nodes O_1, O_2 and O_3 represent the output corresponding to the brain tumor class. A FF-BPNN uses a gradient descent learning algorithm, in which the network weights are moved along the negative of the gradient of the performance function.

The term backpropagation refers to the manner in which the gradient is computed for non-linear multilayer networks.

The proposed network consists of input, hidden and output layer. The input layer is represented by 32 nodes, which have been derived from feature extraction models namely; GLRCM and Gabor techniques. These features are normalized into the values in between 0 and 1. The outputs of each layer are the inputs to the next layer. Ten neurons are in the hidden layer and one neuron in the output layer. Initially the weight and bias are initialized to the values in between -1 and 1. The learning rate is assumed to be 1. The network is trained for the different training data set. The weights and bias are modified during learning process. Finally, the network becomes ready to classify the new data sample. The back propagation algorithm is given below.
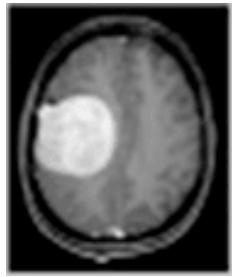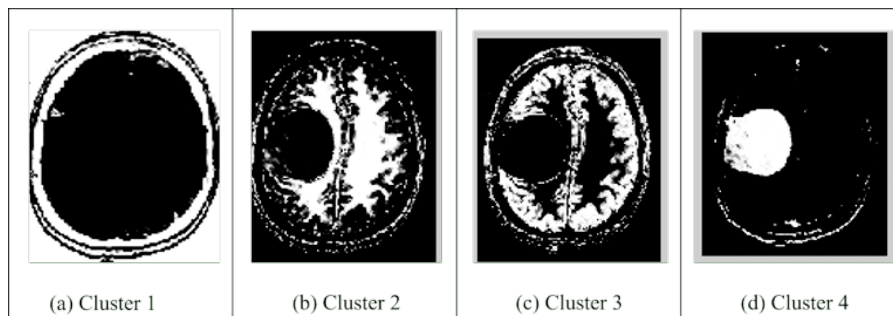
Fig. 4.1: Input Image

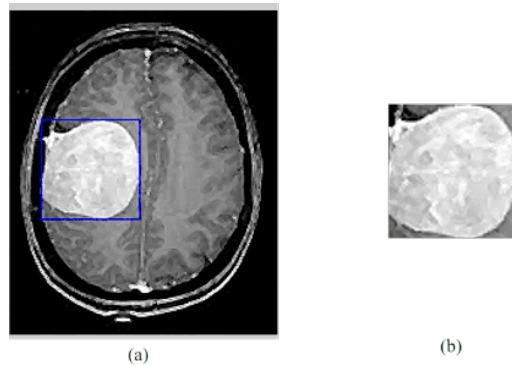Fig. 4.2: Clusters of Input Image given in Figure 4.1.

Fig. 4.3: (a) Tumor Detection & (b) Segmentation of Tumor Region

4. Results and discussion. The data collection in medical image processing [34, 35, 36, 37] plays an important role, So MRI images used in this work were collected from the local hospital. From the collected images, brain tumor is segmented by the method called spatial fuzzy level set segmentation, Gabor features and GLRLM features were extracted from the segmented images.

Considering the input image shown in the above figure, the result of the spatial fuzzy level set segmentation is shown in the figure 4.2.

The tumor region is segmented by using the cluster 4 among the entire four clusters shown in figure 4.3.

The GLRLM and Gabor features are extracted from the segmented image and classified using ANN. The classified result for the above image belongs to the class benign.

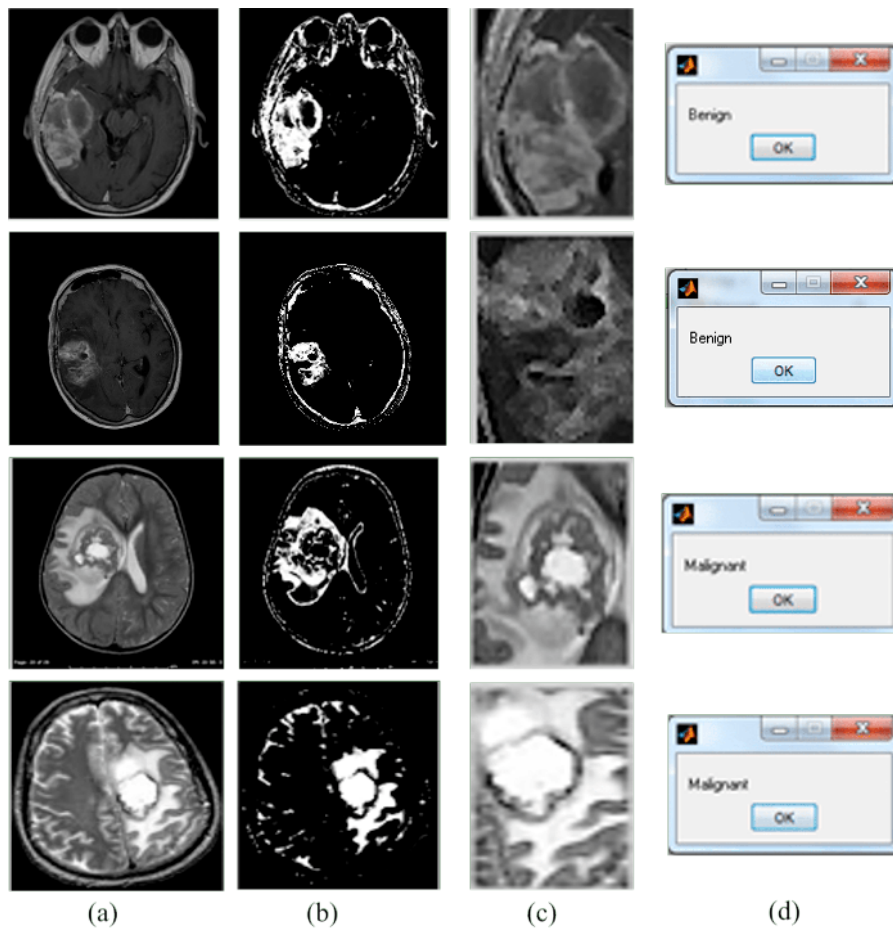Similarly, to the above sample image, the result for other samples is shown in figure 4.4.

Fig. 4.4: (a) Original Image & (b) Selected Cluster & (c) Segmented Image & (d) Classified Result

Table 4.1: Table of Comparison of Accuracy for Segmentation

Sl.No	Authors	Methods	Accuracy
1	Ruchita A et. al [27]	*FCM*	92.67
2	Prof P.Senthil [26]	Level Set Segment	89.99
3	Jason J. Corso Et al [28]	Multilevel Bayesian segmentation	88
4	A R Kavitha and C Chellamuthu [29]	Adaptive Region growing based	46
5	Proposed	Spatial Fuzzy Level Set Segmentation	94

The Comparative Analysis for the Accuracy of Fuzzy based Level Set method with existing segmentation methods are carried out and results are tabulated in Table 4.1.

The Graph consisting of various segmentation methods is plotted with respect to the segmentation accuracy in Figure 4.5.

The bar chart in the Figure 4.5 shows the comparative analysis of five segmentation methods for Accuracy performance parameter. The obtained Accuracy values are 92.67, 89.99, 88, 46, 94 for FCM, Level Set Segment, Multilevel Bayesian segmentation, Adaptive Region growing based and Spatial Fuzzy Level Set Segmentation respectively. From the graphs, the Spatial Fuzzy Level Set Segmentation shows better Accuracy results as
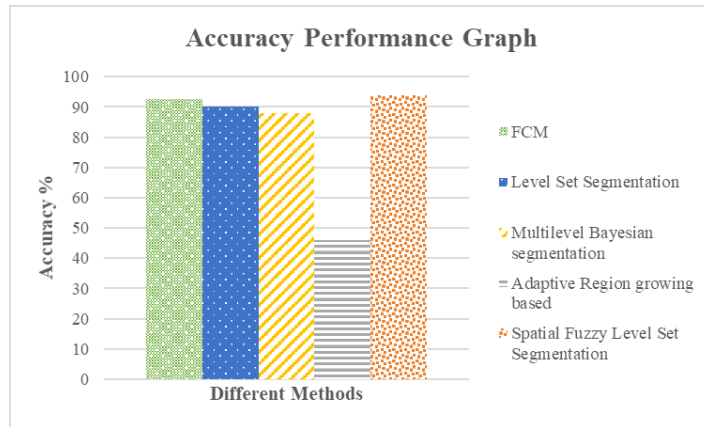
Fig. 4.5: Performance graph of Segmentation methods in terms of Accuracy

Table 4.2: Table for evaluating Sensitivity and Specificity of various Segmentation techniques.

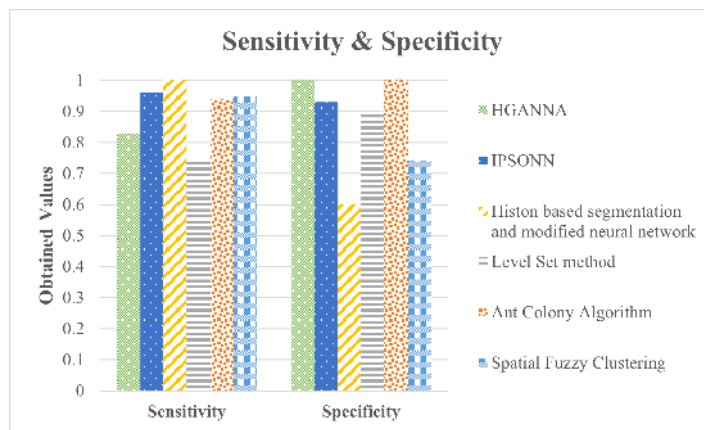| Sl.No	Authors	Methods	Sensitivity	Specificity
1	Sheejakumari V, Gomathi [30]	HGANNA	0.83	1.00
2	Sheejakumari V, Gomathi [31]	IPSONN	0.96	0.93
3	Sheejakumari V, Gomathi [32]	Histon based segmentation and modified neural network	1.00	0.6
4	P.Senthil [26]	Level Set method	0.74	0.90
5	Uttamjeet Kaur [33]	Ant Colony Algorithm	0.94	1.00
6	Proposed work	*Spatial Fuzzy Clustering*	0.95	0.74

Fig. 4.6: Sensitivity and Specificity for Segmentation

compared with other segmentation methods.

The Table 4.2 gives comparison of Sensitivity and specificity for the various segmentation techniques.

Figure 4.6 shows a graph depicting the comparative analysis of various segmentation methods with respect to sensitivity and specificity for segmentation.

Comparative analysis of various classification methods is carried out and the results are tabulated in Ta-

Table 4.3: Comparison Table for existing and Proposed System

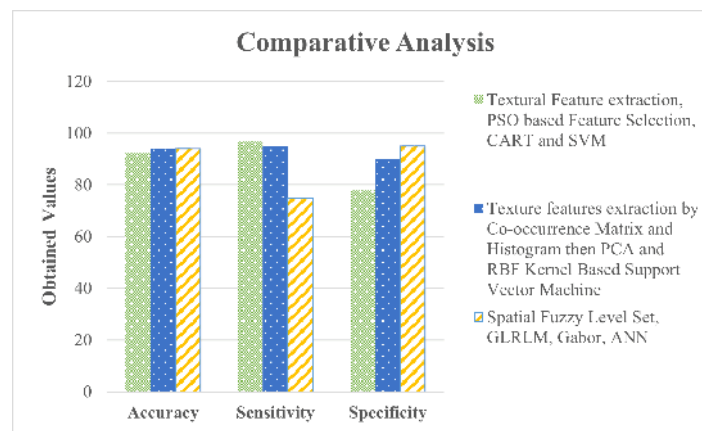| Sl.No	Authors	Methods	Accuracy	Sensitivity	Specificity
1.	Jokin Arul Raj and Sathees Kumar [13]	Textural Feature extraction, PSO based Feature Selection, CART and SVM	92.31	96.67	77.78
2.	P. Kumar and B. Vijayakumar [14]	Texture features extraction by Co-occurrence Matrix and Histogram then PCA and RBF Kernel Based Support Vector Machine	0.94	0.95	0.9
3	Proposed	Spatial Fuzzy Level Set, GLRLM, Gabor, ANN	0.94	0.75	0.95

Fig. 4.7: Performance Graph for Existing and Proposed Methods

ble 4.3.

Finally, bar chart consists of all the parameters such as Accuracy, Sensitivity and Specificity versus three classification systems have been portrayed in Figure 4.7. From the above figure it shows that Proposed computer-aided diagnosis (CAD) system based on Spatial Fuzzy level set with ANN classifier performs well than the other CAD systems as compared in terms of Accuracy and Specificity.

5. Conclusion. The spatial fuzzy technique used in this paper will give more homogeneous regions compared to the other techniques which will eventually help in reducing blur and noisy spots. Level set segmentation is flexible in detecting the edges and has more control on movement of curves. Gabor features are of higher flexibility and represent the images more efficiently by surpassing the directional and Gaussian derivative performances. The higher order statistical texture can be extracted from GLRLM method. By combining these methods, the proposed work gives better results for segmentation and classification with overall classification accuracy of 94%. The accuracy of the proposed method can be improved further by extensive training. In future various state of the art optimization techniques can be used along with ANN classifier in order to increase the accuracy of classification. This CAD system is aimed for the beneficial of radiologist for localization and diagnosis of the brain tumors in the MRI images.

Diagnostic Centre Kalaburagi, for providing MRI images and validating the obtained results.

REFERENCES

[1] POONGODI, M., SHARMA, A., HAMDI, M. ET AL., *Smart healthcare in smart cities: wireless patient monitoring system using IoT*, J Supercomput., 2021.

[2] YONGFU SHAO, JUE WU, HONGPING OU, MIN PEI, LI LIU, ALI AKBAR MOVASSAGH, ASHUTOSH SHARMA, GAURAV DHIMAN, MEHDI GHEISARI, ALIA ASHERALIEVA, *Optimization of Ultrasound Information Imaging Algorithm in Cardiovascular Disease Based on Image Enhancement*, Mathematical Problems in Engineering, 2021, vol. 2021, Article ID 5580630, 13 pages.

[3] DHIMAN, G., VINOTH KUMAR, V., KAUR, A. ET AL, *DON: Deep Learning and Optimization-Based Framework for Detection of Novel Coronavirus Disease Using X-ray Images*, Interdiscip Sci Comput Life Sci, 2021, 13, pp. 260–272.

[4] ERLIN L, MENG W, JIANFENG T, JIANJIAN L, *Automatic Segmentation of Brain Tumor Magnetic Resonance Imaging Based On Multi-Constrains and Dynamic Prior*, Int J Smart Sensing Intell Syst, 2015, 8, pp. 1031-1049.

[5] VIRUPAKSHAPPA AB, *An approach of using spatial fuzzy and level set method for brain tumor segmentation*, International Journal of Tomography & Simulation, 2018, 31 (4).

[6] UPLAONKAR DS, PATIL N, *Modified Otsu thresholding based level set and local directional ternary pattern technique for liver tumor segmentation*, International Journal of System Assurance Engineering and Management, 2022 Jan 13: pp. 1-1.

[7] SAMEENA BANU, AMBIKA, *Segmentation of Brain Tumor Lesion Using the Mumford-Shah Model*, International Journal of Advanced Scientific and Technical Research, 2014, 3 (4), pp. 415-423

[8] SHARMA Y, CHHABRA M. , *An Improved Automatic Brain Tumor Detection System*, Int J Adv Res Comp Sc Soft Eng., 2015, 5, pp. 11–15.

[9] ZHAN T, GU S, FENG C, ZHAN Y, WANG J., *Brain Tumor Segmentation from Multispectral MRIs Using Sparse Representation Classification and Markov Random Field Regularization*, IJIGSP., 2015; 8, pp. 229-238.

[10] BHAWAR KA, BHIL NK., *Brain Tumor Classification Using Neural Network Based Methods*, IJESRT., 2016; 5, pp. 721-727.

[11] APURVA YN, NANDA S., *MRI Brain Tumor Segmentation and Classification based on Multilevel PSVM Classifier*, IRJET., 2016; 3.

[12] SHEEJAKUMARI V, GOMATHI S., *Brain tumor detection from MRI images using Histon based segmentation and modified neural network*, Biomed Res., 2016; S1-S9.

[13] RAJ JA, KUMAR S. *An Enhanced Classifier for Brain Tumor Classification*, IJCTA., 2016; 9, pp. 325-333.

[14] KUMAR P, VIJAYAKUMAR B., *Brain Tumour MRI Segmentation and Classification Using by PCA and RBF Kernel Based Support Vector Machine*, Middle-East J Sci., 2015; 23, pp. 2106-2116.

[15] NITHYAPRIYA G, SASIKUMAR C., *Detection and Segmentation of Brain Tumors using AdaBoost SVM.*, IJIRCCE 2014; 2.

[16] ALFONSE M, BADEEH A., *An Automatic Classification of Brain Tumors through MRI Using Support Vector Machine*, Egyptian Computer Science Journal., 2016; 40.

[17] DEEPA T, MUTHALAGU R, CHITRA K., *MEM Based Brain Image Segmentation and Classification Using SVM*, JEAS., 2015; 10.

[18] NAG M, SHANKER NV., *Image De-Noising By Using Median Filter and Weiner Filter*, IJIRCCE., 2014; 2, pp. 5641-5649.

[19] LI BN, *Integrating spatial fuzzy clustering with level set methods for automated medical image segmentation*, Comput Biol Med., 2011; 41, pp. 1-10.

[20] UMA DEVI N, POONGODI R., *Integration of Spatial Fuzzy Clustering with Level Set for Efficient Image Segmentation*, IJCSCN, 2015; 3, pp. 296-301.

[21] TANG X., *Texture Information in Run-Length Matrices*, IEEE Trans Image Process., 1998; 7.

[22] WIBAWANTO H., *Discriminating Cystic and Non Cystic Mass using GLCM and GLRLM-based Texture Features*, IJEER., 2010; 2, pp. 569-580.

[23] ZHENG D., *Features Extraction Using Gabor Filter Family*, International conference on signal and image processing., 2004; pp. 139-144.

[24] SONI K, KUMA U., *A New Gabor Wavelet Transform Feature Extraction Technique for Ear Biometric Recognition*, IEEE Conference on Power, 2014.

[25] GURLEEN K, HARPREET K., *Efficient Facial Recognition Using PCA-LDA Combination Feature Extraction with ANN Classification*, Int J Adv Res Comp Sci Soft Eng., 2016; 6, pp. 258-263.

[26] SENTHIL P., *Image Mining Base Level Set Segmentation Stages To Provide An Accurate Brain Tumor Detection*, IJECSC., 2016; 6, pp. 8294-8299.

[27] BANCHPALLIWAR RA, SALANKAR SS., *A Review on Brain MRI Image Segmentation Clustering*, IOSR-JECE., 2016; 11, pp. 80-84.

[28] CORSO JJ, SHARON E, DUBE S, EL-SADEN, S, SINHA U, YUILLE A., *Efficient Multilevel Brain Tumor Segmentation with Integrated Bayesian Model Classification*, IEEE Trans Med Imaging., 2011.

[29] KAVITHA AR, Chellamuthu C. *Detection of Brain Tumour from MRI Image using Modified Region Growing and Neural Network*, Imaging Sci J., 2012.

[30] SHEEJAKUMARI V, GOMATHI S., *Healthy and pathological tissues classification in MRI Brain Images using Hybrid Genetic Algorithm-Neural Network (HGANNA) Approach*, EJSR., 2012; 87, pp. 212-226.

[31] SHEEJAKUMARI V, GOMATHI S., *MRI Brain Images healthy and pathological tissue classification with aid of Improved Particle Swarm Optimization and Neural Network (IPSONN)*, Comput Math Methods., 2015; pp. 1-12.

[32] SHEEJAKUMARI V, GOMATHI S., *Brain tumor detection from MRI images using histon based segmentation and modified neural*

network, Biomed Res., 2016.

[33] Kaur U, Sharma R, Dosanjh M., *Cancers Tumor Detection using Magnetic Resonance Imaging with Ant Colony Algorithm*, IJAREEIE, 2016; 4, pp. 58-62.

[34] Veerashetty, S., Virupakshappa & Ambika , *Face recognition with illumination, scale and rotation invariance using multiblock LTP-GLCM descriptor and adaptive ANN*, Int J Syst Assur Eng Manag, 2022.

[35] V.D. Ambeth Kumar, *Medical data mining process using efficient clustering and classification approaches*, International Journal of Innovations in Scientific and Engineering Research, 2020, Vol 7, Issue 8, pp. 106-114.

[36] Virupakshappa, Amarapur B, *An improved segmentation approach using level set method with dynamic thresholding for tumor detection in MRI images*, HELIX. 2017 Jan 1; Vol.7, Issue 5, pp. 2059-66.

[37] T. Jemima Jebaseeli and C. Anand Deva Durai, *A robust ecg signal processing and classification methodology for the diagnosis of cardiac health*, International Journal of Innovations in Scientific and Engineering Research, 2020, Vol 7, Isssue 8, pp.115-123.